Influence of Lateral Constraints on Wave Propagation in Finite Granular Crystals

Hrachya Kocharyan
Department of Mechanical Engineering,
Worcester Polytechnic Institute,
100 Institute Road,
Worcester, MA 01609-2280
e-mail: hkocharyan@wpi.edu

Nikhil Karanjgaokar[1]
Department of Mechanical Engineering,
Worcester Polytechnic Institute,
100 Institute Road,
Worcester, MA 01609-2280
e-mail: nkaranjgaokar@wpi.edu

In the presented work, wave dynamics of 2D finite granular crystals of polyurethane cylinders under low-velocity impact loading was investigated to gain better understanding of the influence of lateral constraints. The deformation of the individual grains in the granular crystals during the impact loading was recorded by a high-speed camera and digital image correlation (DIC) was used to calculate high fidelity kinematic and strain fields in each grain. These grain-scale kinematic and strain fields were utilized for the computation of the intergranular forces at each contact using a granular element method (GEM) based mathematical framework. Since the polyurethane were viscoelastic in nature, the viscoelasticity constitutive law was implemented in the GEM framework and it was shown that linear elasticity using the strain rate-dependent coefficient of elasticity is sufficient to use instead of a viscoelastic framework. These particle-scale kinematic and strain field measurements in conjunction with the interparticle forces also provided some interesting insight into the directional dependence of the wave scattering and attenuation in finite granular crystals. The directional nature of the wave propagation resulted in strong wave reflection from the walls. It was also noteworthy that the two reflected waves from the two opposite sidewalls result in destructive interference. These lateral constraints at different depths leads to significant differences in wave attenuation characteristics and the finite granular crystals can be divided into two regions: upper region, with exponential wave decay rate, and lower region, with higher decay rate. [DOI: 10.1115/1.4047004]

Keywords: granular matter, destructive interference, wave attenuation, impact loading, dynamics, impact, wave propagation

1 Introduction

The investigation of the mechanical wave's propagation through granular media has received considerable research attention during the last few decades. Earlier research reports have shown effects such as wave dispersion [1,2], wave scattering [3], reflection [4], and energy trapping [5]. Based on those and the number of other properties, granular matter can be used in shock absorption and protection layers [6], to build number of devices, e.g., acoustic lenses [7], acoustic switches and logic elements [8], acoustic diodes [9], etc.

Wave propagation through a 1D chain of granular elements is extensively studied in the past both numerically [10–15] and experimentally [4,5,13,16–18]. In the past, numerical studies based on Hertzian contact have been used to prove the existence of solitary waves in granular crystal based on the shape of the velocity of the propagating wave [10]. The binary collision approximation have been used to investigate wave propagation through soft granular chains [11] and wave decay that occurs in various types of tapered granular chains [12,14]. In a recent numerical study [15], it was shown that a local resonator in a granular chain results in quick decrease in propagating wave amplitude. In most of the experiments on the 1D chain of granular elements, the chain is excited from one end, and the propagated wave is recorded at the other end using a strain gauge or by strain gauges placed inside individual particles. These experiments investigate wave propagation at various conditions, using pre-pressed particles or particles without pre-pressing; moreover, the authors compare velocity and force data with theoretical observations made for Hertzian contact [19] and prove the existence of solitary waves predicted by Nesterenko [20] for both chain with pre-compression and without [16]. It was also shown that there is a huge change in reflectivity from the interface of two granular chains [4]. Moreover, it was also shown that there is an energy trapping in tapered chains consisting of particles with high and low elastic moduli [5,13]. In contrast, there are fewer reports of more complicated 2D or 3D case. There are a number of numerical and theoretical studies [21–29], as well as a number of experimental studies [30–33]. Numerical and theoretical methods use meshless techniques such as particle-in-cell technique [22], based on Eulerian and Lagrangian descriptions of materials. However, numerical solution of the Hertzian contact law is a more common technique [21,23,24,26–29]. Experimental studies mostly use photoelasticity to demonstrate wave propagation through 2D granular media and show that the waves travel in the form of solitary waves. Some experiments [32] use strain gauges to measure the forces for various conditions. In various simulations [33,34], contacts are represented using spring-dashpot systems. While this method is quite successful, it has some limitations, e.g., it assumes a constant coefficient of restitution for all velocities [35,36], which is not always accurate [37].

Majority of previous research on wave propagation through granular materials have been using granular materials made of stiff materials, e.g., steel [4,7,32], aluminum [32], etc. However, granular crystals made of soft grains are of high interest too. Number of food products, colloidal suspensions, and microgels are examples of soft granular materials [38]. Wave propagation process is significantly different in soft materials, particularly due to viscoelastic nature of the grains, which results in higher wave absorption [39,40]. Due to this high wave absorption, soft granular materials can have huge potential application in wave traps, protective layers, etc. Soft granular materials are mostly investigated in small deformation regions [41]. Soft granular materials can undergo huge deformation even under small load, which cannot be numerically simulated using Hertzian contact law, due to the limitation of the Hertz' law of less than 5% strain [20]. Some multi-

[1]Corresponding author.

Contributed by the Applied Mechanics Division of ASME for publication in the Journal of Applied Mechanics. Manuscript received February 20, 2020; final manuscript received April 19, 2020; published online May 14, 2020. Assoc. Editor: Yong Zhu.

contact based DEM models have been to describe the deformation of soft granular systems up to 13% strain [42]. However, the utility of multi-contact DEM models can be limited due to the need for accurate experimental calibration for its nondimensional model parameters. This is when methods in discrete (or distinct) element method (DEM) [43] family can be utilized. DEM tracks the movement of individual particles to find contact forces and displacements through expensive computations using Newton's laws based on an apriori assumption of interparticle contact relationship. Since the computational cost for DEM models grows exponentially, these models can become computationally expensive as compared with typical experimental methods and continuum mechanics methods for large granular systems. The DEM-based mathematical framework has also been modified to operate an inverse method to infer interparticle forces for experimental measurements obtained using photoelasticity [30,31,44]. This photoelasticity based visualization of the force chains provide tremendous insight into the mechanics of granular media. However, the photoelasticity based quantitative measurements of interparticle force in granular media have a few limitations, e.g., it requires a birefringent material which should remain elastic throughout the experiment, a priori knowledge of the contact law is needed to quantify the interforces [45]. In order to address these limitations, a new method called granular element method (GEM) [46–48] developed recently can be used to represent strain fields in granular elements and measure interparticle forces. GEM method uses Newton's law of motion and balance of momentum at particle level and an imaging device to track the position of particles. The GEM method will be discussed in more detail in Sec. 2.

In the current paper, the GEM method powered with DIC technique was used to calculate interparticle forces and investigate wave propagation through the granular crystals composed of polyurethane particles. A drop-tower technique was used to load the system and create the propagating wave.

2 Experimental Procedure and Theory

The experimental setup of the drop-tower experiment is shown in Fig. 1(*a*). The experimental procedure was similar to Ref. [49]. Polyurethane (Durometer 80A, McMaster-Carr) cylindrical grains with around 1/2-in. diameter were arranged into a granular crystal in two configurations: body-centered cubic (BCC) and hexagonal close packing (HCP) as shown in Figs. 1(*b*) and 1(*c*). The crystals were put into a fixture with rigid sidewalls and a sliding top wall. The top face size is 4 in., much larger than the particle sizes are. The impactor freely falls under gravity and reaches the fixture holding the granular crystal with about 6 m/s velocity.

The images during the experiment were recorded using a Phantom v710 high-speed camera with frame rates of 4000–8000 fps. A commercial digital image correlation (DIC) software (VIC-2D from Correlated Solutions) were used to calculate displacements and velocities for each grain at any time instant. DIC is an optical technique capable of calculating strains in subpixel range, which measures deformation by tracking gray value pattern on the object's surface. Since DIC requires random, nonrepeating speckle pattern, thus the front face of each grain was patterned using spray paint. Based on the variations of the gray value pattern in each pixel, displacements in horizontal and vertical directions for each pixel were calculated. Using the aforementioned grain-scale displacement fields, in-plane strain fields in each grain were calculated as seen in Fig. 2. It should be noted that the strain fields shown in Fig. 2 are based on DIC analysis performed for each grain independently in order to obtain better accuracy for

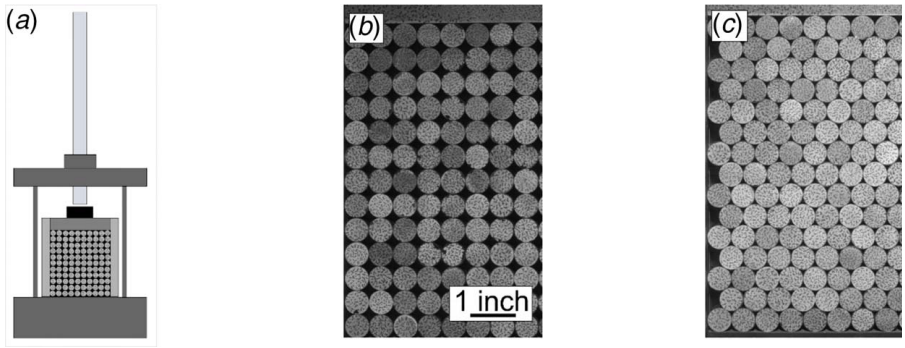

Fig. 1 (*a*) The experimental setup and left half of the granular crystals in (*b*) BCC and (*c*) HCP configurations

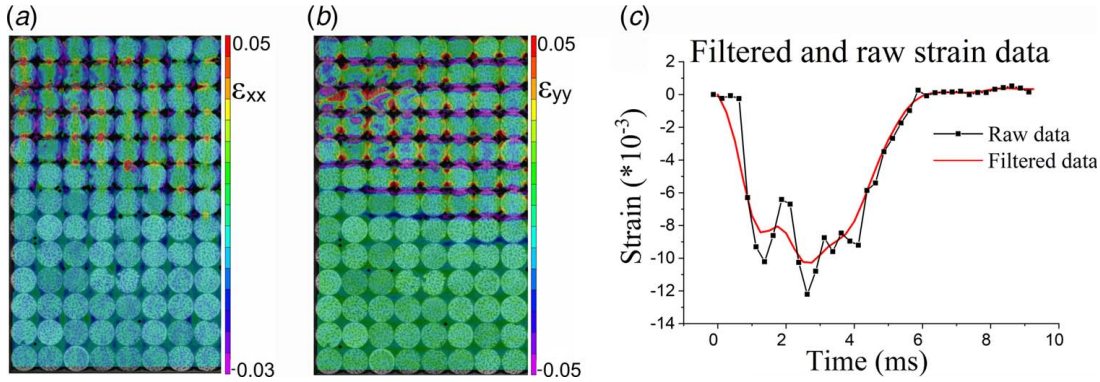

Fig. 2 (*a*) Horizontal and (*b*) vertical strain fields obtained by DIC for the particles in the BCC system and (*c*) a typical example of a filtered and raw ε_{yy} strain signal

kinematic and strain field measurements. Using a surface averaging approach for displacement (u,v) and in-plane strain fields (ε_{xx}, ε_{yy}, and ε_{xy}) at various time instants, the average displacement, strain, velocity, and acceleration were computed in each grain for every time instant. The high frequency noise in these "raw" volume averaged strain and kinematic measurements was eliminated using a moving average filter. An example of typical "raw" volume averaged strain signal ε_{yy} strain and its filtered version is represented in Fig. 2(*c*). The error between the raw signal and filtered signal was monitored for each strain and kinematic quantity for each grain to make sure that the filtered signal truly represents the raw experimental data. The significant advantage of using DIC over other techniques, e.g., using strain gauges is that in every particle, on average 20*20 or 400 data readings were computed with a displacement resolution ~0.05–0.1 pixel. Moreover, an accuracy of 0.1% was assumed for the displacements, which, along with the imaging framerate can be used to calculate velocities and accelerations numerically.

The grain-scale kinematic and strain measurements were then used to compute the interparticle force chains in the finite granular crystals at any time instant using a modified GEM approach, described below. GEM is an advanced inverse numerical technique in DEM family introduced recently by Andrade and Avila [46], which combines an imaging technique to collect experimental data, with a mathematical framework to solve the interparticle force problem. GEM method uses grain level strain values and kinematic data (particle displacements and material fabric) as an model input to numerically solve the governing equations. The conservation of linear and angular momentums as well as the balance between external forces and stresses inside each particle are considered to be the governing laws in GEM mathematical framework. Using a multiobjective optimization approach, the experimental data in conjunction with the mathematical framework can be used to infer the interparticle forces at every contact in the granular system. The aforementioned matthematical framework used in the current work is described below.

The law for conservation of linear and angular momentums are given as [47]

$$\frac{d}{dt}\int_{V_p}\rho\mathbf{v}dV=\int_{V_p}\rho\mathbf{b}dV+\int_{\delta V_p}\mathbf{t}dS \tag{1}$$

$$\frac{d}{dt}\int_{V_p}\mathbf{x}\times\rho\mathbf{v}dV=\int_{V_p}\mathbf{x}\times\rho\mathbf{b}dV+\int_{\delta V_p}\mathbf{x}\times\mathbf{t}dS \tag{2}$$

where ρ is the material density, $\mathbf{v}$ is the velocity, V_p is the particle volume, $\mathbf{b}$ is the body force, t are surface tractions, and $\mathbf{x}$ is the position vector. Taking the derivatives and ignoring the body forces, as well as rewriting this for the mass center

$$\sum_{c=1}^{N_C}f^c=m_p a_p^{cm} \tag{3}$$

$$\sum_{c=1}^{N_C}x^c\times f^c=m_p(x_p^{cm}\times a_p^{cm}) \tag{4}$$

where x^c and f^c are contacts' position vectors and contact forces, respectively. Equations (3) and (4) for all particles can be combined into a matrix to form an objective function $K_m\cdot f=D_m$.

Using strain field data, stress fields can be calculated using $\bar{\bar{\sigma}}=C*\bar{\bar{\varepsilon}}$, where C is the stiffness tensor. Volume averaged stress can be calculated from the stress field using [47]

$$\bar{\sigma}_p=\frac{1}{V_p}\int_{V_p}\sigma dV \tag{5}$$

Left multiplying by the identity matrix, using divergence theorem, the balance of linear momentum, neglecting the body forces and writing Eq. (5) for the mass center

$$\sum_{c=1}^{N_c}x^c\otimes f^c=V_p\bar{\sigma}_P+m_p(x_p^{cm}\otimes a_p^{cm}) \tag{6}$$

which again can be combined into a matrix to form another objective function $K_s\cdot f=D_s$.

Coulomb-type friction and cohesionless interaction are assumed as constraints and using two objective functions, the interparticle forces can be inferred by a multiobjective optimization process, which can be found in Ref. [50].

In a typical GEM framework, a linear elastic constitutive response was used for each grain in the granular system. However, since in the current research soft, viscoelastic polyurethane grains were used, there is a need to adopt the viscoelastic effect in the mathematical framework. For this purpose, dynamic mechanical analysis (DMA) of polyurethane (Durometer 80A, McMaster-Carr) sheet was performed. The dynamic response for the polyurethane material was modeled as a Prony series with two time constants and a mathematical representation of the time-dependent relaxation modulus was found to be

$$E(t)=15.7+253.1\cdot e^{-t/2.64}+1320.4\cdot e^{-t/0.55}\ \text{(MPa)} \tag{7}$$

where time constants 2.64 and 0.55 are in seconds.

As it will be shown later, the duration of the experiment was about 5–6 ms, which, as it can be seen from Eq. (7), is about two orders of magnitude less than the time constants of the relaxation modulus, meaning that the viscoelastic creep is negligible, and the stress fields can be calculated from the strain fields directly using the relaxation modulus. In Sec. 3, it will be shown that due to the short duration of the experiment, stress calculation can be simplified even further, and a linear elastic law can be used, where the "effective" coefficient of elasticity can be calculated from the Prony series using strain rate in the particle. In order to find the "effective" coefficient of elasticity, the framework from Pacheco et al. [51] was implemented. According to Ref. [51], stress can be expressed as

$$\sigma^{\text{Prony}}=\dot{\varepsilon}\sum_{q=1}^{\text{TN}}E_q\int_0^t e^{-(t-\tau)/\tau_q}d\tau \tag{8}$$

where $\dot{\varepsilon}$ is the strain rate, E_q and τ_q are qth Maxwell model components, while TN is the total number of those components, which in our case is two. Using the obtained stress, stress–strain curve can be plotted, and the "effective" coefficient of elasticity can be obtained from the graph.

3 Results and Discussions

Interparticle force change over time for four different contacts can be seen in Fig. 3. In Figs. 3(*b*)–3(*e*), it can be seen that there are two—red and black curves, where the black curve represents the force calculated using viscoelastic relaxation modulus in GEM, while the red curve represents the force calculated using linear elasticity law with an "effective" coefficient of elasticity. In DMA, relaxation modulus is calculated by applying varying stress and for each stress, calculating the coefficient of elasticity. The "effective" coefficient of elasticity, calculated using the method discussed in Sec. 2, was found to be about 150 MPa, 530 MPa, 740 MPa, and 480 MPa for the top particle in contact 1, the left particles in contacts 2, 3, and the particle in contact 4, respectively. As already mentioned, these values were calculated using strain rates in each particle. Due to the nature of the experiment, as obtained strain and strain rates are very noisy, containing high frequency noise, thus the lowpass function of MATLAB with a normalized passband frequency of 0.3 was used. Despite the high image acquisition framerates, some minimal motion blur was observed for the top two rows for the first image recorded post-

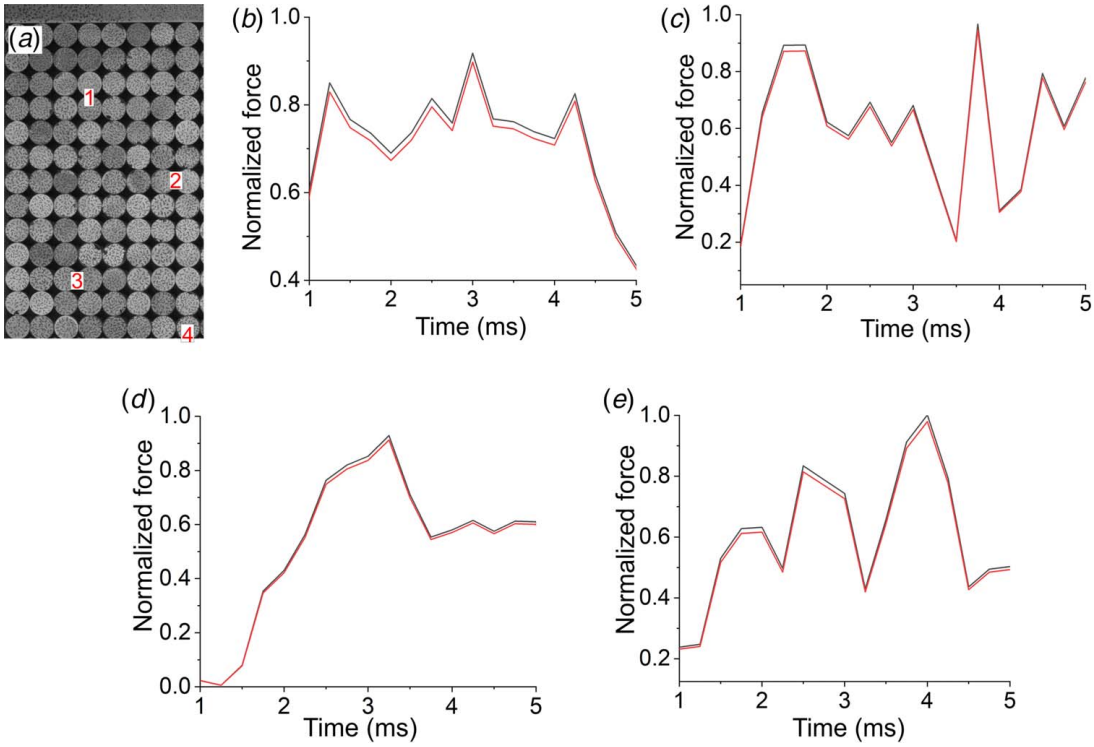

Fig. 3 (*a*) BCC system with numbered contacts and corresponding force versus time plots of (*b*) contact 1, (*c*) contact 2, (*d*) contact 3, and (e) contact 4, where the black curve represents force calculated using the viscoelastic relaxation modulus, whereas the red curve represents force calculated using "effective" coefficient of elasticity (Color version online.)

impact. Thus, a moving average approach was used to smoothen strain rate data for the grains in the top two rows to eliminate the overestimation of strain rates for this first time instant after the initial impact. In order to determine the difference between the black and red curves, the force curves can be integrated over time, which will represent the momentum. After integration, it was found that the difference between the viscoelastic and elastic laws for the particles presented is in order of 1.65–2.2%. As it can be seen visually from Fig. 3 and quantitatively from the above values, the difference between the viscoelastic and the linearly elastic frameworks is negligibly small, meaning that a simpler linearly elastic framework along with the "effective" coefficient of elasticity is adequate for the calculation of the interparticle forces. This framework will be used below to calculate forces (presented in Fig. 7) acting on the particles when the initial wave reaches them and to prove the effect of lateral constraint on wave propagation.

The lateral displacement plots (transverse to the direction of the vertical impact) for a simple BCC ordered polyurethane granular system at different time instances are plotted in the Fig. 4. Lateral displacement of the particles will be discussed in detail, as it has a huge effect on the vertical wave motion, which will be proved below. As it can be seen from Fig. 4, in all images until when the system relaxes in Fig. 4(*e*), the two parts of the image are almost perfectly symmetric. To take advantage of this symmetry, in all our further discussions, only a half of the system was considered for the data analysis through DIC, as this will provide a much higher temporal resolution for DIC based kinematic and strain measurements for the same system size and the imaging system. However, this procedure involves the inherent assumption of midplane symmetry for the granular system and may introduce some uncertainty in our analysis. While the uncertainty introduced by the assumption of symmetry may affect the individual measurements, these would not significantly influence the spatial distribution of the full-field kinematic and strain fields.

As seen in Fig. 5, at the time instance corresponding to Fig. 5(*a*), upper few grains have negative displacement, i.e., they move toward the rigid wall on the left. Due to symmetry, the upper few grains in right half of the finite granular crystal (not shown here) would move in the opposite direction toward the rigid wall on the right. Thus, the upper few rows of this finite granular crystal experience a tensile lateral load at this particular time instant. This is a result of the incident wave traveling away from the center toward the wall.

At the time instant corresponding to Fig. 5(*b*), the incident wave passed the upper few layers and now reached few layers below. Since the incident wave passed the upper layers, they begin to return back to their original position and have positive velocity, thus they move away from the wall. Thus, these upper few layers would experience a net compressive load in the lateral direction. In Figs. 5(*c*)–5(*e*), a similar trend can be seen with the only difference that the incident wave dies down with depth. Moreover, it can be seen that the reflected wave is moving toward the center of the image. Due to symmetry, the two reflected waves from two walls reach each other at the same time and phase at around seven grain layers and a destructive interference happens, i.e., the reflected waves cancel each other, as it can be seen in Fig. 5(*f*). Similar interference effect [1,3,9] and destructive interference of waves [52] have been previously reported for granular matter. A very comparable image can be seen for the HCP ordered polyurethane granular crystal (see Fig. 6). Comparing with the BCC system, as it can be seen, wall neighboring particles in the HCP system differ from the rest of the granular crystal. This is because of huge rotational motion of the grains near the wall in this case resulting from the configurational features of the system. Due to the large displacement in the finite HCP crystals, the grains near walls tend to undergo huge in-plane rotations as evidenced in these plots. However, despite these differences for grains close to the walls, a destructive interference similar to the BCC system occurs in these HCP finite granular crystals when the reflected waves from walls

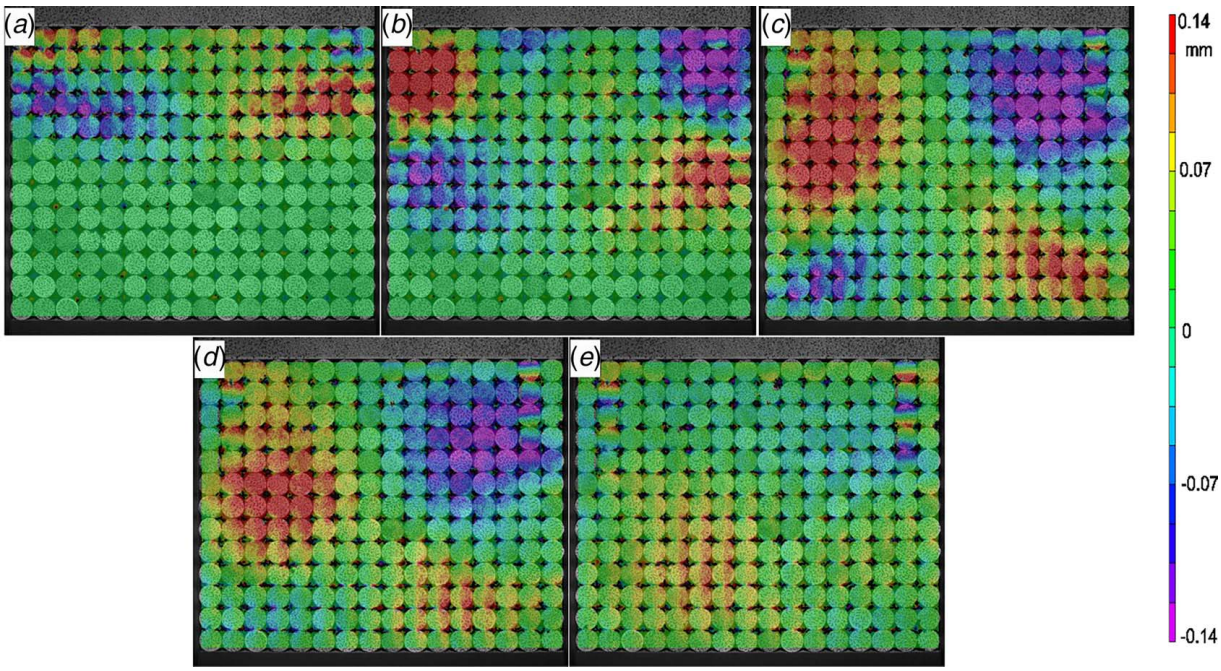

Fig. 4 Horizontal displacement plots of full-sized BCC ordered system at (*a*) 1 ms, (*b*) 1.5 ms, (*c*) 2.25 ms, (*d*) 2.75 ms, and (*e*) 3 ms

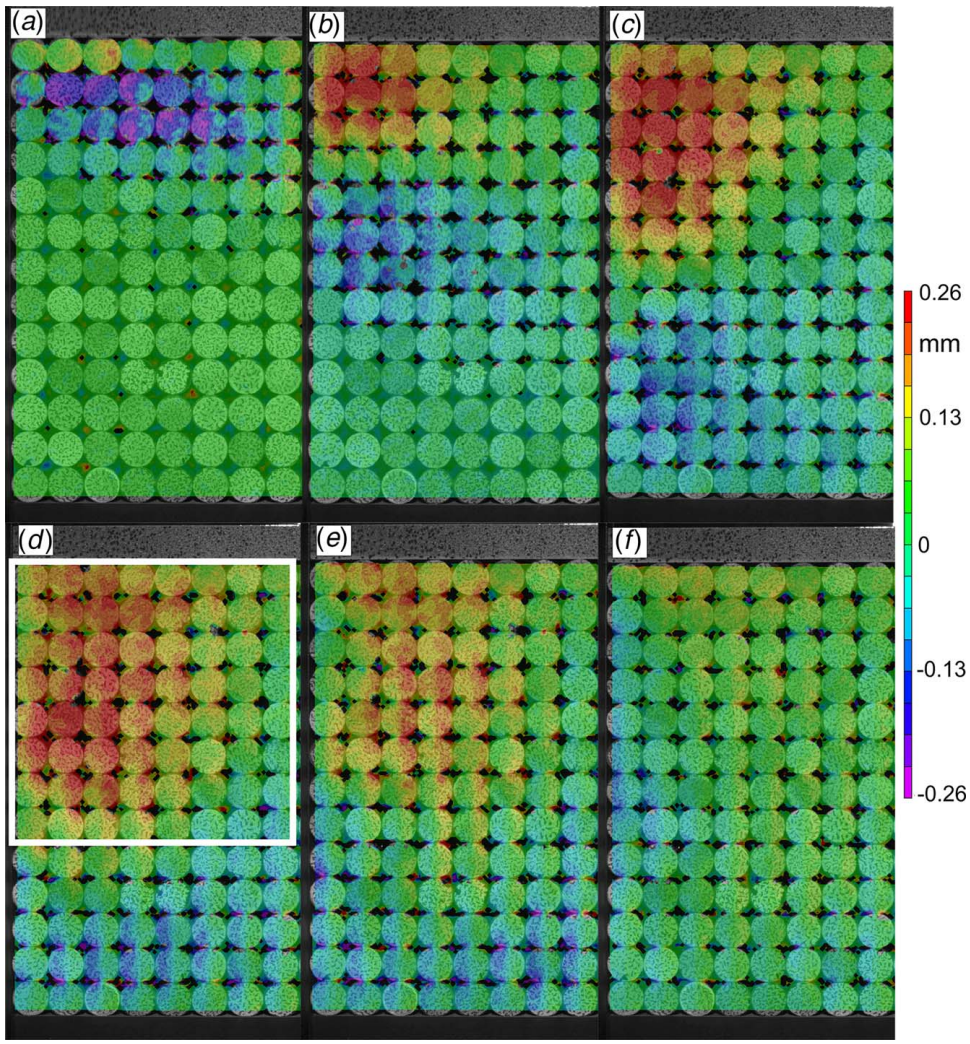

Fig. 5 Horizontal displacement plots of BCC ordered system at (*a*) 0.75 ms, (*b*) 1.25 ms, (*c*) 1.75 ms, (*d*) 2.25 ms, (*e*) 2.5 ms, and (*f*) 2.75 ms

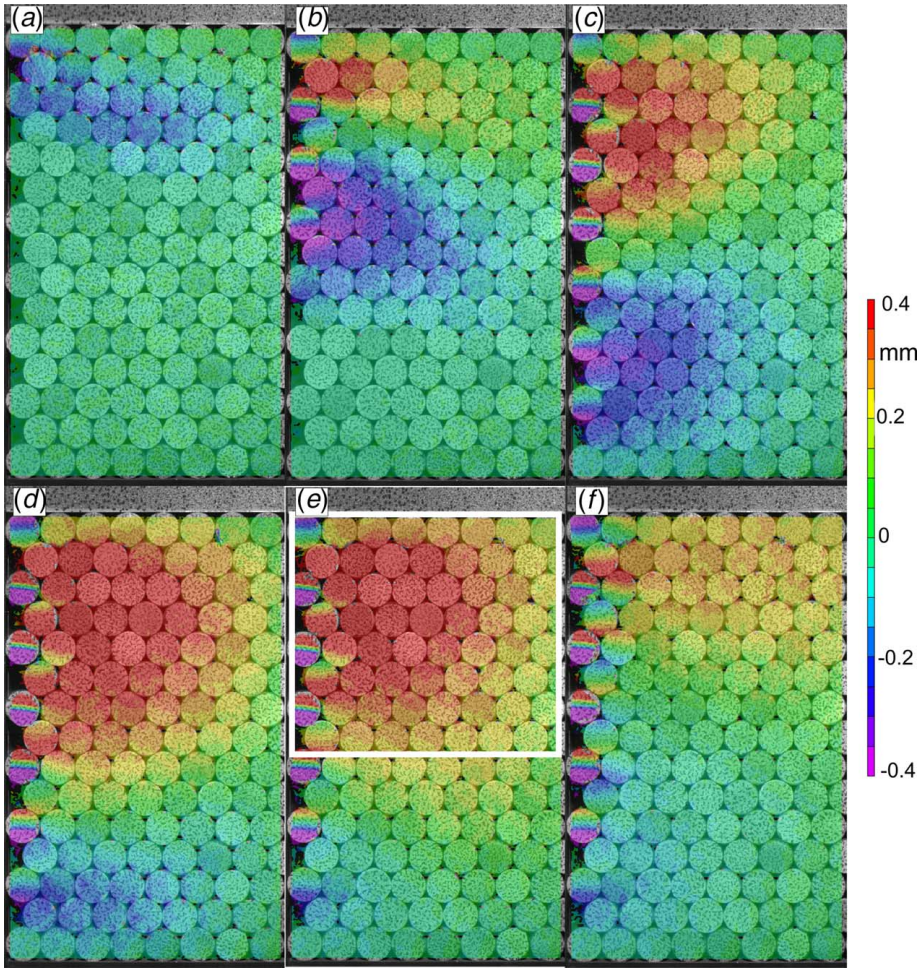

Fig. 6 Horizontal displacement plots of HCP ordered system at (*a*) 0.75 ms, (*b*) 1.25 ms, (*c*) 1.75 ms, (*d*) 2.25 ms, (e) 2.75 ms, and (*f*) 3.25 ms

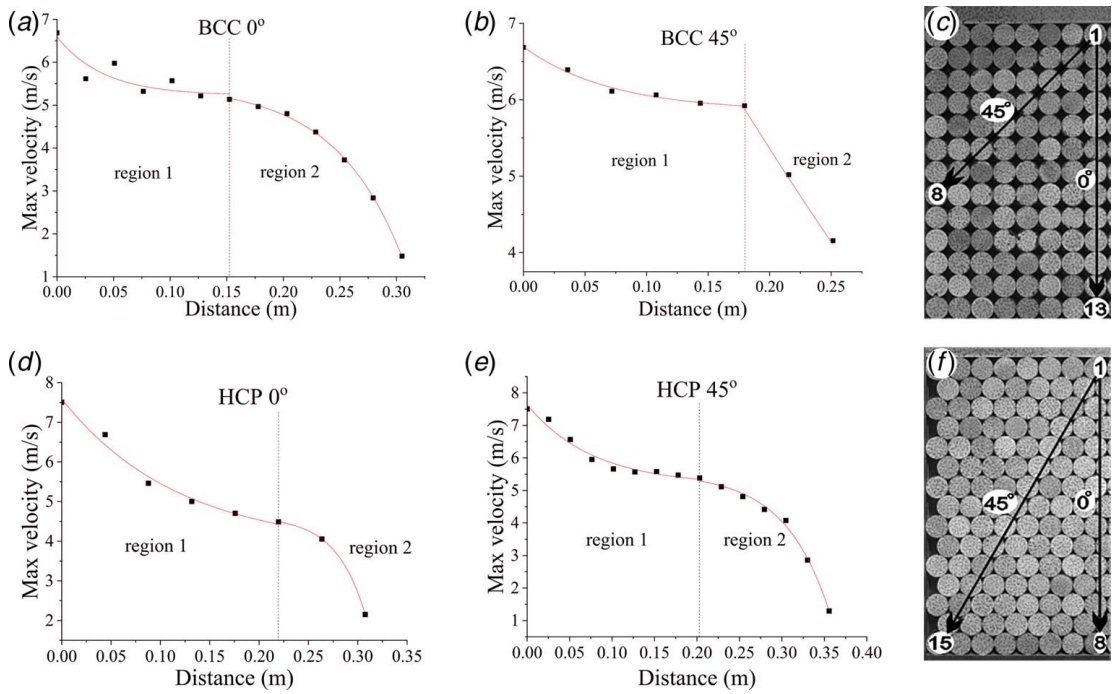

Fig. 7 Maximum velocity of the particles with depth for BCC system at (*a*) 0 deg and (*b*) 45 deg and HCP system at (*d*) 0 deg and (e) 45 deg with corresponding angles and directions for (c) BCC and (*f*) HCP crystals

reach each other at approximately 8–9 grain layers. This interference effect results in different lateral constraints for the upper part and lower layers of the finite granular crystals and plays a major role on the wave propagation in these finite crystals. It was also observed that the influence of reflected wave, like the primary wave, is directional in nature.

Considering the sizes of both crystals, it can be seen that the depth at which the destructive interference happens depends on the transverse size of the system, i.e., the reflected wave is limited to a "square" area on the top of the system (see Fig. 6(*e*)). This is an important result, indicating that the depth where most of the kinetic energy in concentrated can be modified by changing the lateral size of the system or external lateral constraints in the form of external loading in the lateral direction.

In Fig. 7, plots for the maximum velocity of the grains at various depths are represented for both crystals at two different angles—along vertical and diagonal directions. For simplicity, these directions will be labeled as 0 deg and 45 deg. As it can be seen, the plots can be divided into two distinct regions. In the first region of the plot, the amplitude of maximum velocity for the grains decreases exponentially as function of the depth, however, in the second part, the amplitude of the maximum velocity decreases at a much higher rate. This behavior is consistent for both BCC and HCP crystals for both directions. Moreover, it can be seen that the depth at which the second part of the graph begins occurs at around the same depth as the destructive interference of two reflected waves shown earlier in Figs. 5 and 6. This behavior can be attributed to different lateral constraints experienced by the two upper and lower parts of the granular crystals. In the upper region, where the reflected wave is present, the grains are under lateral compression at the instant of maximum velocity along the longitudinal direction. Thus, the wave propagation through the grains follows a wave decay law like continuous media, i.e., the amplitude decreases exponentially in this region. This kind of exponential decay has been previously reported for the granular matter [27–29] and it was explained that the exponential decay region corresponds to a low-disorder system. The reason for exponential decay is explained for example in Refs. [20,27]. The equation of motion of the *i*th particle in a granular chain is routinely described as [20]

$$m_i\ddot{u}_i = A[(u_{i+1} - u_i)^{3/2} - (u_i - u_{i-1})^{3/2}] \tag{9}$$

where $A = E\sqrt{2R}/3(1-\nu^2)$ and the solution of this equation is an exponential function.

As opposed to this, where there is no compressive lateral force or it is significantly smaller in the lower region, the particles are free to vibrate, thus have higher disorder and transfer only fraction of the wave that reaches them. Huge energy loss here can be a result of much more friction between particles, as well as multiple scattering events. The particles in this region behave more individually comparing with the upper part of the finite granular crystals. This is a very important result, which shows that by varying the size of the system, more specifically the transverse size, it is possible to control the depth where most of the impact is concentrated. In order to investigate the influence of particle stiffness and particle size, similar impact experiments were conducted for BCC and HCP granular crystals consisting of (1) polycarbonate grains with ½ in. diameter and (2) polyurethane grains with 1 in. diameter. The wave propagation characteristics for finite granular crystals with both the larger polyurethane grains and stiffer polycarbonate grains exhibited very similar trends with two distinct regions, upper region with exponential wave decay and lower region with higher rate decay.

The spatial wave decay rate in region 1 of different finite granular systems would be assessed using an exponential fitting in the form of $\exp(-\alpha^* x)$, where α is the coefficient of attenuation or the decay rate and x is the distance from the point of initial impact. The coefficient of attenuation represents the reciprocal of the distance over which wave amplitude decreases by a factor of e (Euler's constant). Thus, a larger value for the coefficient of attenuation would indicate a faster spatial decay rate for wave amplitude as the wave propagates through a medium. Since the coefficient of attenuation is only applicable for exponential spatial decay, the coefficient of attenuation was calculated only for the region 1. It should be noted that the coefficient of attenuation was not calculated for region 2 as the spatial wave decay rate in this region varies significantly from an exponent decay. From the data fitting in Fig. 7, the coefficient of attenuation in the finite granular crystals was found to be around 1.6–1.8 m^{-1}, with HCP crystals having a slightly higher coefficient of attenuation. In both the BCC crystals along 45 deg as well as HCP crystals at 0 deg, the attenuation coefficient is drastically different, which is a result of a limited number of particles in these directions; however, the general behavior is reproducible.

Above, when discussing the velocity behavior (thus the kinetic energy), it was assumed that the presence of two regions with different decays was a result of different lateral forces. In Fig. 8, lateral forces for both the finite granular crystals along the longest directions are shown for the instant when the initial wave reaches the particle (i.e., velocity is maximum). Forces for two other directions discussed above show a similar trend as those in Fig. 8, however, due to a limited number of particles, are not as representative, so it will not be included in this discussion. As it can be seen from Fig. 8, lateral forces show a similar trend as the velocities. It can be seen, that there are two regions with slightly different forces. In the first region, the forces are higher, whereas there is a sudden drop in force values in the second region. The borderline between these two regions is at approximately the same height where it was identified for the velocities in Fig. 7. This proves the previous claim about lateral compression affecting the wave propagation. As it can be seen from Fig. 8, force data is noisier

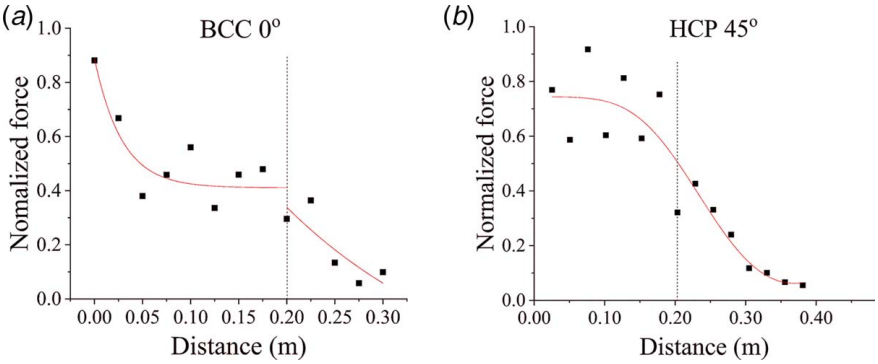

Fig. 8 Lateral forces when the initial wave reaches the particles (*a*) BCC system along 0 deg direction and (*b*) HCP system along 45 deg direction

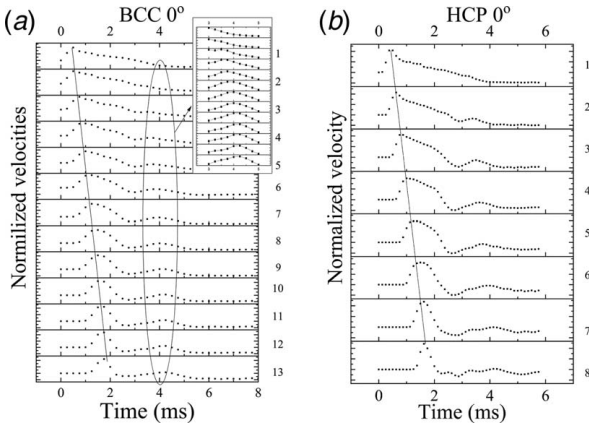

Fig. 9 Velocity versus time plots of the particles along the 0 deg for (*a*) BCC and (*b*) HCP systems

than the velocity data, which is a result of more complicated calculations involved in the GEM-based force calculations, as well as more complicated wave processes and interactions between the particles. It should be noted that the force values in Fig. 8 are not necessarily the maximum force values in the particle but are instantaneous force values when initial wave passes through the particle.

The velocities of grains along 0 deg in both BCC and HCP finite granular crystals are shown in Fig. 9. As it can be seen from Fig. 8, in both BCC and HCP crystals, there is a huge peak in the beginning and a much smaller peak later at around 4 ms. The first peak corresponds to the primary wave, whereas the second small peak is due to reflected waves. This assumption was made based on the fact that the second peak appears at some certain depth only and cannot be found for first few particles. As it is shown in Fig. 9 by a solid line, the wave is traveling along the system and reaches each next particle after some delay. Using this information, the velocity of the wave propagation or the time-of-flight velocity was estimated to be around 125 m/s and has no detectable dependence on the system size or the direction of propagation. It should be noted that this is an average velocity over the whole system, and it is not necessarily equal to local wave propagation velocity over the whole duration of the experiment, which is a function of local instantaneous force [20] and is not the group velocity, which was found to differ significantly due to nonlinearity and coupling of nonlinearity with dispersion [53]. Moreover, in both granular crystals, it can be seen that the primary wave broadens with depth and begins to narrow again at some point. Wave broadening effect in granular media was observed in earlier reports [54,55]. This change in wave broadening behavior happens at around the same depth where the reflected waves were reaching each other and was connected with the effect of constraint change already mentioned above and seen in Figs. 5 and 6. The broadening of the wave in the upper part of the system, where most of the impact was localized, meaning that the energy of the impulse becomes more distributed over the time and thus the potential damaging effect of the impulse is reduced. However, both reports mentioned [54,55] agree that the wave broadening happens in high disorder system too and that the wave decay follows a power law, i.e., it is faster than exponential, which was already observed in Fig. 7. This does not match with what can be seen in the bottom half of Fig. 9. As it can be seen, the wave narrows down after initial broadening. In comparison with the current experiment, both [54] and [55] use granular crystals with a huge number of particles. Ref. [54] represents a numerical simulation of elastic granular gas, whereas [55] experimentally investigates various elastic and viscoelastic, highly disordered granular crystals. The limitation of Ref. [55] is that it measures the bulk wave that reached the bottom of the system and has no information on the particle level. For viscoelastic material, the authors report wave broadening similar to elastic granular crystals; however, they did not consider varying lateral compression, which was found to affect the wave width [56].

Figure 10 shows the probability distribution of maximum velocities of all particles in both BCC and HCP systems. Although some previous results [57–59] show deviation from Gaussian $\sim\exp(v/v_0)^2$ distribution toward $\sim\exp(v/v_0)^{1.5}$, thus Gaussian is unsuccessful in predicting high and low velocities, as it can be seen from Fig. 10, the distribution in both of the systems is very close to a Gaussian distribution. However, it should be noted that the papers above report distribution in granular media consisting of glass beads [57], granular gas with a huge number of particles [58], and the velocity statistics for granular media consisting of viscoelastic grains are absent from the literature. In Ref. [59], the authors report theoretical calculations of velocity distribution using the spring-dashpot model to represent the nonlinear contacts in granular media. The authors found Gaussian distribution in a low dissipation system, whereas for higher dissipation system the distribution becomes closer to $\sim\exp(v/v_0)^{1.5}$ form.

As it can be seen from Fig. 10, there is a slight difference between the distribution plots of BCC and HCP systems. As it can be seen, the HCP system has lower variance comparing with BCC system, which results in higher probability of the mean value of maximum velocities and lower spread of the maximum velocity values. In the smaller velocity region, a discrete group of particles can be seen, which likely represents the lowest row of the system, where besides the fact that velocity is naturally very small, it is also affected by the rigid floor. At high-velocity region, neglecting one point in HCP, which is likely an error, BCC configuration has a higher concentration of high-velocity particles.

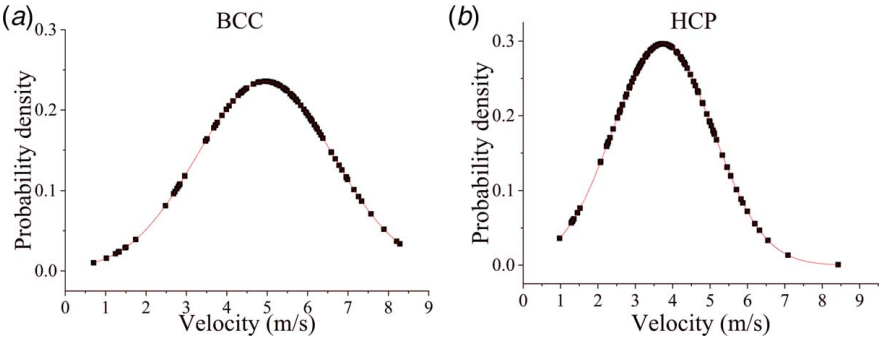

Fig. 10 Maximum velocity probability distribution plots of all particles in BCC (*a*) and HCP (*b*) systems. The dots show experimental results and the solid line is the Gaussian fitting.

4 Conclusions

In this study, experimental investigation of the wave propagation through the system of granular particles was presented. The viscoelastic framework was discussed, and it was shown that for experiments with short duration, the viscoelastic framework can be successfully substituted by linear elastic framework using the strain rate-dependent coefficient of elasticity. It was found that in the granular systems with finite sizes, the wave propagation process is governed by effects due to the finite sizes of the system and that there is a huge reflection from the walls. Analyzing the observed destructive interference, it was found that the transverse size of the granular system defines the depth where most of the impact is concentrated, thus by varying the size of the system, it is possible to control the wave propagation process. It was also found, that due to destructive interference, based on the wave attenuation behavior, the system can be divided into two parts: upper, with exponential wave decay rate, and lower, with higher decay rate. The exponential decay is likely a result of particles being under lateral compression by the reflected wave, which does not reach the lower part and the particles here have no or much less lateral compression, which have been proved to be correct as well. This less compression results in a much higher rate of wave attenuation. In the exponential decay part, significant broadening of the propagating wave was observed, resulting in energy being more distributed over time. In addition, despite other researchers found a deviation from Gaussian distribution, it was found that Gaussian distribution successfully predicts the velocity distributions in the system.

Acknowledgment

The authors would also like to acknowledge the financial support through Worcester Polytechnic Institute startup funds. In particular, the authors would like to express their gratitude to the NSF-MOMS program and the program managers Dr. Qidwai and Dr. Goulbourne for the funding support through the NSF CAREER award # 1845200.

References

[1] Doney, R. L., Agui, J. H., and Sen, S., 2009, "Energy Partitioning and Impulse Dispersion in the Decorated, Tapered, Strongly Nonlinear Granular Alignment: A System With Many Potential Applications," J. Appl. Phys., **106**(6), p. 064905.
[2] Thomas, C. N., Papargyri-Beskou, S., and Mylonakis, G., 2009, "Wave Dispersion in Dry Granular Materials by the Distinct Element Method," Soil Dyn. Earthquake Eng., **29**(5), pp. 888–897.
[3] Martínez, A. J., Yasuda, H., Kim, E., Kevrekidis, P. G., Porter, M. A., and Yang, J., 2016, "Scattering of Waves by Impurities in Precompressed Granular Chains," Phys. Rev. E, **93**(5), p. 052224.
[4] Nesterenko, V. F., Daraio, C., Herbold, E. B., and Jin, S., 2005, "Anomalous Wave Reflection at the Interface of Two Strongly Nonlinear Granular Media," Phys. Rev. Lett., **95**(15), p. 158702.
[5] Daraio, C., Nesterenko, V. F., Herbold, E. B., and Jin, S., 2006, "Energy Trapping and Shock Disintegration in a Composite Granular Medium," Phys. Rev. Lett., **96**(5), pp. 1–15.
[6] Fraternali, F., Porter, M. A., and Daraio, C., 2008, "Optimal Design of Composite Granular Protectors," Mech. Adv. Mater. Struct., **17**(1), p. 13.
[7] Spadoni, A., and Daraio, C., 2010, "Generation and Control of Sound Bullets With a Nonlinear Acoustic Lens," Proc. Natl. Acad. Sci. U. S. A., **107**(16), pp. 7230–7234.
[8] Li, F., Anzel, P., Yang, J., Kevrekidis, P. G., and Daraio, C., 2014, "Granular Acoustic Switches and Logic Elements," Nat. Commun., **5**(1), p. 5311.
[9] Boechler, N., Theocharis, G., and Daraio, C., 2011, "Bifurcation-Based Acoustic Switching and Rectification," Nat. Mater., **10**(9), pp. 665–668.
[10] Chatterjee, A., 1999, "Asymptotic Solution for Solitary Waves in a Chain of Elastic Spheres," Phys. Rev. E **59**(5), pp. 5912–5919.
[11] Rosas, A., and Lindenberg, K., 2004, "Pulse Velocity in a Granular Chain," Phys. Rev. E—Stat. Nonlin. Soft Matter Phys., **69**(3), pp. 2–4.
[12] Harbola, U., Rosas, A., Esposito, M., and Lindenberg, K., 2009, "Pulse Propagation in Tapered Granular Chains: An Analytic Study," Phys. Rev. E—Stat. Nonlin. Soft Matter Phys., **80**(3), pp. 1–10.
[13] Porter, M. A., Daraio, C., Herbold, E. B., Szelengowicz, I., and Kevrekidis, P. G., 2008, "Highly Nonlinear Solitary Waves in Periodic Dimer Granular Chains," Phys. Rev. E—Stat. Nonlin. Soft Matter Phys., **77**(1), pp. 1–4.
[14] Lindenberg, K., Harbola, U., Romero, H., and Rosas, A., 2011, "Pulse Propagation in Granular Chains," AIP Conference Proceedings, Lake Louise, Alberta, Canada, Sept. 20–24, pp. 97–110.
[15] Vorotnikov, K., Starosvetsky, Y., Theocharis, G., and Kevrekidis, P. G., 2018, "Wave Propagation in a Strongly Nonlinear Locally Resonant Granular Crystal," Phys. D Nonlin. Phenom., **365**, pp. 27–41.
[16] Coste, C., Falcon, E., and Fauve, S., 1997, "Solitary Waves in a Chain of Beads Under Hertz Contact," Phys. Rev. E, **56**(5), pp. 6104–6117.
[17] Daraio, C., Nesterenko, V. F., Herbold, E. B., and Jin, S., 2005, "Strongly Nonlinear Waves in a Chain of Teflon Beads," Phys. Rev. E, **72**(1), p. 016603.
[18] Carretero-González, R., Khatri, D., Porter, M. A., Kevrekidis, P. G., and Daraio, C., 2009, "Dissipative Solitary Waves in Granular Crystals," Phys. Rev. Lett., **102**(2), pp. 1–4.
[19] Nesterenko, V. F., 1984, "Propagation of Nonlinear Compression Pulses in Granular Media," ASME J. Appl. Mech. Tech. Phys., **24**(5), pp. 733–743.
[20] Nesterenko, V. F., 2001, *Dynamics of Heterogeneous Materials*, Springer New York, New York, NY.
[21] Herrmann, H. J., and Luding, S., 1998, "Modeling Granular Media on the Computer," Continuum Mech. Thermodyn., **10**(4), pp. 189–231.
[22] Bardenhagen, S. G., and Brackbill, J. U., 1998, "Dynamic Stress Bridging in Granular Material," J. Appl. Phys., **83**(11), pp. 5732–5740.
[23] Bouchaud, J. P., Claudin, P., Levine, D., and Otto, M., 2001, "Force Chain Splitting in Granular Materials: A Mechanism for Large-Scale Pseudo-Elastic Behaviour," Eur. Phys. J. E, **4**(4), pp. 451–457.
[24] Awasthi, A. P., Smith, K. J., Geubelle, P. H., and Lambros, J., 2012, "Propagation of Solitary Waves in 2D Granular Media: A Numerical Study," Mech. Mater., **54**, pp. 100–112.
[25] Xu, J., and Zheng, B., 2016, "Stress Wave Propagation in Two-Dimensional Buckyball Lattice," Sci. Rep., **6**(1), p. 37692.
[26] Awasthi, A., Wang, Z., Broadhurst, N., and Geubelle, P., 2015, "Impact Response of Granular Layers," Granul. Matter, **17**(1), pp. 21–31.
[27] Manciu, M., Sen, S., and Hurd, A. J., 2001, "Impulse Propagation in Dissipative and Disordered Chains With Power-Law Repulsive Potentials," Phys. D Nonlin. Phenom., **157**(3), pp. 226–240.
[28] Harbola, U., Rosas, A., Romero, A. H., and Lindenberg, K., 2010, "Pulse Propagation in Randomly Decorated Chains," Phys. Rev. E, **82**(1), p. 011306.
[29] Hong, J., 2005, "Universal Power-Law Decay of the Impulse Energy in Granular Protectors," Phys. Rev. Lett., **94**(10), pp. 18–21.
[30] Shukla, A., and Damania, C., 1987, "Experimental Investigation of Wave Velocity and Dynamic Contact Stresses in an Assembly of Disks," Exp. Mech., **27**(3), pp. 268–281.
[31] Shukla, A., 1991, "Dynamic Photoelastic Studies of Wave Propagation in Granular Media," Opt. Lasers Eng., **14**(3), pp. 165–184.
[32] Burgoyne, H. A., Newman, J. A., Jackson, W. C., and Daraio, C., 2015, "Guided Impact Mitigation in 2D and 3D Granular Crystals," Proc. Eng., **103**, pp. 52–59.
[33] Tanaka, K., Nishida, M., Kunimochi, T., and Takagi, T., 2002, "Discrete Element Simulation and Experiment for Dynamic Response of Two-Dimensional Granular Matter to the Impact of a Spherical Projectile," Powder Technol., **124**(1–2), pp. 160–173.
[34] Maknickas, A., Kačeniauskas, A., Kačianauskas, R., Balevičius, R., and Džiugys, A., 2006, "Parallel DEM Software for Simulation of Granular Media," Informatica, **17**(2), pp. 207–224.
[35] Tsuji, Y., Kawaguchi, T., and Tanaka, T., 1993, "Discrete Particle Simulation of Two-Dimensional Fluidized Bed," Powder Technol., **77**(1), pp. 79–87.
[36] Schwager, T., and Pöschel, T., 2007, "Coefficient of Restitution and Linear–Dashpot Model Revisited," Granular Matter, **9**(6), pp. 465–469.
[37] Wu, C., Li, L., and Thornton, C., 2003, "Rebound Behaviour of Spheres for Plastic Impacts," Int. J. Impact Eng., **28**(9), pp. 929–946.
[38] Menut, P., Seiffert, S., Sprakel, J., and Weitz, D. A., 2012, "Does Size Matter? Elasticity of Compressed Suspensions of Colloidal- and Granular-Scale Microgels," Soft Matter, **8**(1), pp. 156–164.
[39] Restrepo, D., Mankame, N. D., and Zavattieri, P. D., 2015, "Phase Transforming Cellular Materials," Extreme Mech. Lett., **4**, pp. 52–60.
[40] Shan, S., Kang, S. H., Raney, J. R., Wang, P., Fang, L., Candido, F., Lewis, J. A., and Bertoldi, K., 2015, "Multistable Architected Materials for Trapping Elastic Strain Energy," Adv. Mater., **27**(29), pp. 4296–4301.
[41] Harada, S., Takagi, S., and Matsumoto, Y., 2003, "Wave Propagation in a Dynamic System of Soft Granular Materials," Phys. Rev. E—Stat. Nonlin. Soft Matter Phys., **67**(6), p. 061305.
[42] Brodu, N., Dijksman, J. A., and Behringer, R. P., 2015, "Multiple-Contact Discrete-Element Model for Simulating Dense Granular Media," Phys. Rev. E—Stat. Nonlin. Soft Matter Phys., **91**(3), pp. 1–6.
[43] Cundall, P. A., and Strack, O. D. L., 1979, "A Discrete Numerical Model for Granular Assemblies," Géotechnique, **29**(1), pp. 47–65.
[44] Lesniewska, D., and Wood, D. M., 2009, "Observations of Stresses and Strains in a Granular Material," J. Eng. Mech., **135**(9), pp. 1038–1054.
[45] Clark, A. H., Kondic, L., and Behringer, R. P., 2012, "Particle Scale Dynamics in Granular Impact," Phys. Rev. Lett., **109**(23), p. 238302.
[46] Andrade, J. E., and Avila, C. F., 2012, "Granular Element Method (GEM): Linking Inter-Particle Forces With Macroscopic Loading," Granular Matter, **14**(1), pp. 51–61.
[47] Hurley, R., Marteau, E., Ravichandran, G., and Andrade, J. E., 2014, "Extracting Inter-Particle Forces in Opaque Granular Materials: Beyond Photoelasticity," J. Mech. Phys. Solids, **63**(1), pp. 154–166.
[48] Hurley, R. C., Hall, S. A., Andrade, J. E., and Wright, J., 2016, "Quantifying Interparticle Forces and Heterogeneity in 3D Granular Materials," Phys. Rev. Lett., **117**(9), p. 098005.

[49] Karanjgaokar, N., 2017, "Evaluation of Energy Contributions Using Inter-Particle Forces in Granular Materials Under Impact Loading," Granular Matter, **19**(2), p. 36.
[50] Hurley, R. C., Lim, K. W., Ravichandran, G., and Andrade, J. E., 2016, "Dynamic Inter-Particle Force Inference in Granular Materials: Method and Application," Exp. Mech., **56**(2), pp. 217–229.
[51] Pacheco, J. E. L., Bavastri, C. A., and Pereira, J. T., 2015, "Viscoelastic Relaxation Modulus Characterization Using Prony Series," Lat. Am. J. Solids Struct., **12**(2), pp. 420–445.
[52] Alagoz, S., and Baykant Alagoz, B., 2013, "Sonic Crystal Acoustic Switch Device," J. Acoust. Soc. Am., **133**(6), pp. EL485–EL490.
[53] Liu, C., and Nagel, S. R., 1993, "Sound in a Granular Material: Disorder and Nonlinearity," Phys. Rev. B, **48**(21), pp. 15646–15650.
[54] Somfai, E., Roux, J.-N., Snoeijer, J., van Hecke, M., and van Saarloos, W., 2005, "Elastic Wave Propagation in Confined Granular Systems," Phys. Rev. E, **72**(2), p. 021301.
[55] Langlois, V., and Jia, X., 2015, "Sound Pulse Broadening in Stressed Granular Media," Phys. Rev. E, **91**(2), p. 022205.
[56] Santibanez, F., Zuñiga, R., and Melo, F., 2016, "Mechanical Impulse Propagation in a Three-Dimensional Packing of Spheres Confined at Constant Pressure," Phys. Rev. E, **93**(1), p. 012908.
[57] Losert, W., Cooper, D. G. W., Delour, J., Kudrolli, A., and Gollub, J. P., 1999, "Velocity Statistics in Excited Granular Media," Chaos Interdiscip. J. Nonlin. Sci., **9**(3), pp. 682–690.
[58] Herrmann, H. J., Luding, S., and Cafiero, R., 2001, "Dynamics of Granular Systems," Phys. A Stat. Mech. Appl., **295**(1–2), pp. 93–100.
[59] Bray, D. J., Swift, M. R., and King, P. J., 2007, "Velocity Statistics in Dissipative, Dense Granular Media," Phys. Rev. E, **75**(6), p. 062301.